applied optics

Model-based restoration using light vein for range-gated imaging systems

Canjin Wang,* Tao Sun, Tingfeng Wang, Rui Wang, Jin Guo, and Yuzhen Tian

State Key Laboratory of Laser Interaction with Matter, Changchun Institute of Optics, Fine Mechanics and Physics, Chinese Academy of Science, Changchun 130033, China
**Corresponding author: wcjpsh@126.com*

Received 30 June 2016; revised 8 August 2016; accepted 10 August 2016; posted 10 August 2016 (Doc. ID 269505); published 6 September 2016

The images captured by an airborne range-gated imaging system are degraded by many factors, such as light scattering, noise, defocus of the optical system, atmospheric disturbances, platform vibrations, and so on. The characteristics of low illumination, few details, and high noise make the state-of-the-art restoration method fail. In this paper, we present a restoration method especially for range-gated imaging systems. The degradation process is divided into two parts: the static part and the dynamic part. For the static part, we establish the physical model of the imaging system according to the laser transmission theory, and estimate the static point spread function (PSF). For the dynamic part, a so-called light vein feature extraction method is presented to estimate the fuzzy parameter of the atmospheric disturbance and platform movement, which make contributions to the dynamic PSF. Finally, combined with the static and dynamic PSF, an iterative updating framework is used to restore the image. Compared with the state-of-the-art methods, the proposed method can effectively suppress ringing artifacts and achieve better performance in a range-gated imaging system.

OCIS codes: (110.4850) Optical transfer functions; (110.1080) Active or adaptive optics; (010.3310) Laser beam transmission; (010.7295) Visibility and imaging.

http://dx.doi.org/10.1364/AO.55.007229

1. INTRODUCTION

Range-gated imaging systems are normally used in low light scenes, such as underwater and at night. The imaging quality is reduced by backscattering, speckle noise, imaging jitter, atmospheric turbulence, etc. Better visibility is required by the following target recognition and tracking. Therefore, it is necessary to carry out research on image restoration technology for range-gated imaging systems.

The goal of image restoration is to recover a sharp image according to some prior of the imaging process (e.g., the PSF of the system, the distribution of noise), which plays an important role in many image processing tasks. Traditional restoration methods include iterative blind deconvolution (IBD), non-negativity and support constraint recursive inverse filtering (NAS-RIF), Wiener Filtering, etc. These methods perform well in some cases with sufficient illumination and abundant imaging details. However, with the decrease of details and contrast, these approaches perform poorly in laser active imaging.

In recent years, a large number of scholars have done significant research in image restoration and many algorithms and frameworks have been proposed. Cai *et al.* [1] normalized the kernel under a tight-wavelet framework and proposed an adaptive split Bregman method to solve the energy function. Cho and Lee [2] extracted image structure through strong edges for establishing the regularization equation and achieved a fast restoration speed. Krishnan *et al.* [3] presented a low-complexity method which maintained the high-frequency component of the image by constructing a scale invariant regularization sparse equation. Fergus *et al.* [4] constructed a joint posterior probability function between the latent and degraded image, then maximized the function to calculate the blur kernel. Shan *et al.* [5] proposed a local smoothing approach applied in low-contrast regions to suppress ringing artifacts. Xu *et al.* [6] constructed a new l0 sparse expression and applied it into a MAP framework. They achieved a good restoration performance for noisy images without an extra filtering process. Yuan *et al.* [7] estimated the blur kernel with two images, and put forward a secondary deconvolution approach to remove ringing artifacts brought by single deconvolution. Goldstein and Fattal [8] proposed a whitening spectrum formula to estimate the spectrum distribution of the fuzzy kernel. Tai and Lin [9] proposed a blind deconvolution algorithm for iterative restoration of noisy images. These above approaches normally estimate blur kernel using edge, texture, or gradient, so that in conditions of adequate illumination and sharp texture, they can obtain good performance. However, in laser active imaging it is difficult to accurately extract edge or texture details because of the poor illumination. On the other hand, speckle noise would

introduce artificial edges, which leads to larger errors in blur kernel estimation.

In this paper, a novel model-derived approach based on the static and dynamic degradation PSF of the imaging system is established. First, considering beam propagation, diffraction limit, and other individual components, the physical model of the imaging system is established to estimate the static PSF. Second, a light vein feature extraction method is proposed to estimate dynamic PSF. Finally, according to the blur model of range-gated imaging systems, the two PSFs are applied into an iterative restoration framework based on expectation maximization (EM) algorithm. In the experiment part, the comparison with state-of-the-art approaches proved the validity of our algorithm.

2. IMAGING MODEL

The schematic diagram of our range-gated imaging system is shown in Fig. 1, which consists of three parts: a laser emitting device, an optical imaging system (optical lens and intensified charge-coupled device, ICCD), and a range-gated control board. The optical axis of the laser is parallel to that of the ICCD. The light source is a diode-pumped solid pulse laser with a laser pulse width of 8 nS, wavelength of 532 nm, and single pulse energy ranges from 10 to 40 mJ. In order to suppress the backscattered light and increase the detection range, a pulse sequence generator is used to control the opening and closing of the ICCD gate.

The Gaussian beam from the pulsed laser belongs to a spherical wave. Due to the imaging range, which is far greater than the Rayleigh length $Z = \pi\omega_0^2/\lambda$, the laser can be regarded as a point light source. The transmission of the laser beam is as follows: emitted by the laser, passed through the atmosphere, reflected by the object, then into the lens and arrived at the ICCD's imaging plane.

The goal of our static imaging model is to estimate the static point spread function of the imaging system, so that we can predict the intensity of each pixel according to the source power, reflectance properties of targets, sensor characteristics, and other factors. According to the transmission path in Fig. 1, we proposed an imaging model suitable for imaging system in atmosphere. The flowchart of our method is shown in Fig. 2.

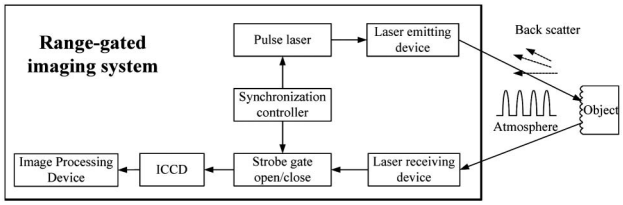

Fig. 1. Schematic diagram of range-gated imaging system.

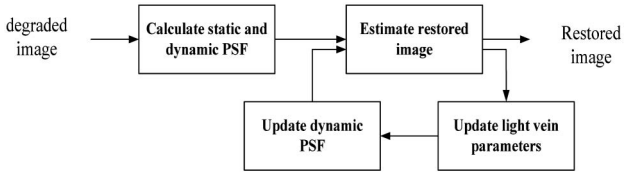

Fig. 2. Flowchart of the proposed method.

The analysis of image degradation involves noise, atmospheric attenuation, atmospheric turbulence, system distortion, diffraction limit, platform vibration, and many other reasons. In this paper, we divided them into two parts: static ones and dynamic ones. The static factors are relatively stable during the imaging, while the dynamic factors keep changing among each frame. In the next section we try to analyze and model the two parts.

3. ESTIMATION OF STATIC PSF

In this section, the static imaging process is modeled and its PSF is established by the transmission path of the light. Generally speaking, the modulation transfer function (MTF) of the whole static imaging system is composed of the MTF of the atmosphere, the MTF of the diffraction limit, and the MTF of the sensor.

A. MTF of Atmosphere

According to [10,11], the light energy E_{rcv} received by the ICCD consists mainly of three parts, which are target-reflected light E_d, forward-scattered light E_f, and backscattered light E_b, respectively, as is expressed in Eq. (1):

$$E_{\text{rcv}} = E_d + E_f + E_b. \tag{1}$$

The target-reflected light exponentially decayed in the transmission path. Regarding the target as a Lambert emitter, E_d can be calculated as

$$E_d(x,y) = \frac{n^2 P_0 T_1 T_2 \rho D^2 \cos^3\varphi \cos^4\varphi'}{16\pi l_d^2 f^2 \sin^2\left(\frac{\alpha}{2}\right) \exp[k l_d(\sec\varphi + \sec\varphi')]}, \tag{2}$$

where n denotes the refractive index of the atmosphere; P_0 denotes the output peak power of the laser; T_1 and T_2 are, respectively, the optical transmittance of the laser transmitting and receiving system; ρ denotes the average reflectivity of the target; D denotes the receiving aperture of the optical system; k denotes the attenuation coefficient of the atmosphere; l_d denotes the transmission distance of the reflected light; f denotes the focal length of the receiving optical system; α denotes the divergence angle of the expanding laser; $\varphi = \arccos\left[l_d/\sqrt{(x+d_0)^2 + y^2 + l_d^2}\right]$; $\varphi' = \arccos\left[l_d/\sqrt{x^2 + y^2 + l_d^2}\right]$; and (x, y) denotes the coordinates on the ICCD imaging plane. The attenuation coefficient in the atmosphere is related to factors such as molecular absorption, molecular scattering, atmospheric aerosol absorption, and atmospheric aerosol scattering, and is sensitive to changes of altitude, weather, temperature, and humidity. It is difficult to accurately model the attenuation coefficient. In this paper, the atmospheric attenuation coefficient k is considered as a constant during the experiment because of the relatively stable environment.

The forward-scattered light is the light reflected by the target and arriving at the ICCD through the atmosphere, which can be calculated as

$$E_f(x,y) = \left[\frac{e^{-Gl_f} - e^{-kl_f}}{e^{-kl_f}} \times E_d(x,y,l_f)\right] * g(x,y,l_f), \tag{3}$$

where $g(x,y,l_f)$ denotes the atmospheric point spread function, which can be calculated as $g(x,y,l_f) = F^{-1}(e^{-Bl_f f_\theta}) / \iint F^{-1}(e^{-Bl_f f_\theta})\mathrm{d}x\mathrm{d}y$; $f_\theta = l_f \times \sqrt{f_x^2 + f_y^2}$

denotes the angular frequency; and l_f denotes the transmission distance of the forward-scattered light. The forward-scattered light carries the information of the target surface, but it would decrease the contrast of the image.

The backscattered light is the part of the light which returns to the ICCD during the path to the target because of atmospheric scatter. It will interfere with the target-reflected light. Although the effect of backscattered light can been effectively suppressed by range-gated technology, for the accuracy of the model, it is significant to calculate the backscattered light received during the opening of the gating. By the theory based on time integral, the energy of the backscattered light can be calculated as

$$E_b(x,y) = \frac{\pi\beta P_0 T_1 T_2 d_R^2 n^2 (1+\cos\theta_s)}{4c^2 t^2 \sum d_p(x,y)} \exp(-2kl_b), \quad (4)$$

where $d_p(x,y)$ denotes the pixel size of the sensor, l_b denotes the transmission distance of the backscattered light, and d_R denotes the radius of the receiving optical system.

The MTF of the atmospheric transmission is defined as the ability to reproduce the target information in the process of transmission. Since the reflected light and forward-scattered light carry the information of the target, while the backscattered light overwhelms the target information, the MTF of the atmospheric transmission is defined as

$$\mathrm{MTF}_{\mathrm{atmosphere}} = \frac{\pi}{4} F\left(\frac{E_d + E_f}{E_d + E_f + E_b}\right). \quad (5)$$

B. MTF of Diffraction Limit

Due to the limitations of the aperture of optical system, the diffraction limit of the imaging system [12,13] needs to be considered as a factor of image degradation, and the MTF is

$$\mathrm{MTF}_{\mathrm{diffraction}} = \frac{2}{\pi}\left[\arccos\frac{f_{\mathrm{so}}}{f_{\mathrm{co}}} - \frac{f_{\mathrm{so}}}{f_{\mathrm{co}}}\sqrt{1-\left(\frac{f_{\mathrm{so}}}{f_{\mathrm{co}}}\right)^2}\right], \quad 0 < f_{\mathrm{so}} < f_{\mathrm{co}}, \quad (6)$$

where f_{so} denotes the spatial frequency, and f_{co} denotes the cutoff frequency of the imaging plane.

C. MTF of the Sensor

The projection of the object on the ICCD plane is distorted, which is mainly determined by the pixel size. The MTF is expressed as

$$\mathrm{MTF}_{\mathrm{distorted}} = \frac{\sin(\pi f_{\mathrm{se}} d_p)}{\pi f_{\mathrm{se}} d_p}, \quad (7)$$

where f_{se} and d_p denote the spatial frequency and the pixel size of the ICCD, respectively.

D. Static PSF of the Imaging System

Considering the factors discussed above, the static MTF of the imaging system can be calculated as

$$\mathrm{MTF}_{\mathrm{static}} = \mathrm{MTF}_{\mathrm{atmosphere}} \cdot \mathrm{MTF}_{\mathrm{diffraction}} \cdot \mathrm{MTF}_{\mathrm{distorted}}. \quad (8)$$

Due to the circular symmetry of the optical device, the PSF of the whole system can be calculated by a one-dimensional integral, which is described in [14]:

$$\mathrm{PSF}_{\mathrm{static}}(\theta) = 2\pi \int J_0(2\pi\theta f_s)\mathrm{MTF}(f_s) f_s \mathrm{d}f_s, \quad (9)$$

where J_0 denotes the Bessel function, f_s denotes the spatial frequency in cycles per radian, and θ denotes the offset with respect to the optical axis.

4. ESTIMATION OF DYNAMIC PSF

In the airborne laser imaging system, atmospheric disturbance and relative motion between the targets and the optical system are also two components that are responsible for image degradation. Due to the randomness and complexity of the turbulence and mechanical vibration, the degradation details by these two factors keep changing during the imaging process, and we can hardly establish a constant physical model. Therefore, it is necessary to determine the two factors for a single image separately.

In this section, we put forward an approach to extract the characteristic of the so-called light vein features from the image, which are useful for estimating the dynamic PSF.

A. Light Vein

Definition: due to source jitter, defocus, and atmospheric disturbance, some veins which are normally brighter than the target and background would appear in the imaging plane. We simply name them light veins. A light vein is like the moving trail of the point source. Using those veins that are generated by small enough light spots, the blur kernel of image motion can be estimated.

The light vein regions meeting our requirements should have some particular properties. The gray values in those areas are relatively larger; some areas are even allowed to be saturated. The highlight pixels are closely distributed with long, thin stripes and relatively sharp edges. With the exception of light veins, the rest of the sections which belong to the background are clean enough. The light vein regions with the above properties contain less noise, which are suitable for estimating an accurate motion trajectory.

In this paper, we propose a method to extract the light vein patterns based on a multiscale pyramid, which consists of the following steps.

(1) Convolve the image with a Gaussian kernel and build a n-layer scale pyramid.

(2) Divide each layer of the pyramid into $s \times t$ small blocks with overlapping. For each block, convert it into a binary image Q_{ij} using Otsu's method with a threshold T_{ij}, where $i = 1, \ldots, n$ is the index of layers, $j = 1, \ldots s \times t$ is the block index in each layer.

(3) Add up the number of pixels with a gray value of 1 in each block, which is labeled as N_{ij}. Assuming that the total number of pixels in Q_{ij} is NT_{ij}, if N_{ij}/NT_{ij}, <20%, go ahead and jump to step (4). Otherwise, it means that the stripe is too thick or has too much noise, and the block is discarded.

(4) Assuming that P_{ij} is the block corresponding to Q_{ij} in the degraded image, with a size of $a_{ij} \times b_{ij}$. In the sub-block with a size of $a_{ij}/2 \times b_{ij}/2$ located in the center of P_{ij}, search for the pixel with the maximum gray value, which is labeled as $(x\max_{ij}, y\max_{ij})$. Starting from $(x\max_{ij}, y\max_{ij})$ in Q_{ij}, extend along the direction of the pixel gray value of 1 to both ends, and

add up the number of pixels to NR_{ij}. If the extending path is beyond the boundary of the block, which means that the block does not contain the entire light vein, discard the block. If $NR_{ij}/N_{ij} < 50\%$, which means there is too much noise or more than one light vein in the block; discard these blocks as well.

(5) Interpolate the eligible blocks to calculate the corresponding location and size in the degraded image and we get the candidate light vein $\varphi = \{Ct(x_{ij}, y_{ij}), W_{ij}, H_{ij}\}$, where Ct, W_{ij} and H_{ij} denotes the center, width, and height of the candidate patch.

After getting the candidate light vein patches, we need to find the best light vein P_b. Then P_b is used to estimate the dynamic blur kernel.

The light veins can be considered as the trajectories of small light spots. With little noise, the histograms of the candidate patches are similar. Therefore, we proposed a light vein selecting method: calculating the gradient histograms of all patches in φ, and clustering the histograms using a K-means algorithm. After a few number of iterations, similar histograms are divided into the same cluster and different histograms are separated, which ends up with a group of clusters $\phi = \{P_0, P_1, \ldots\}$. Selecting the cluster with maximum members, denoted as P_i, and calculating the local contrast of each patch in P_i, we considered the patch with the largest contrast as the best light vein patch P_b.

B. Estimating Dynamic PSF using the Best Light Vein Patch

In order to estimate the blur kernel (dynamic PSF) in every single frame, we use the framework in [2] and define an energy function f_{h_d} as

$$f_{h_d}(h_d) = \sum_{(x,y)\in \mathrm{rem}} \omega_* \|h_d * P_* - g_*\|^2 + \alpha\|h_d\|^2 + \beta \sum_{(x,y)\in P_b} \|S_b * h_d - P_b\|^2, \tag{10}$$

$$(P_*, g_*) = \{(P_x, \partial_x g), (P_y, \partial_y g), (\partial_x P_x, \partial_{xx} g), (\partial_y P_y, \partial_{yy} g), ((\partial_x P_y + \partial_y P_x)/2, \partial_{xy} g)\}, \tag{11}$$

where $\omega_* = \{\omega 1, \omega 2\}$ is a constant coefficient matrix, $S_b(r_b, l_b)$ denotes the source spot which generates p_b; r_b denotes the radius of S_b; l_b denotes the gray value of S_b; h denotes the dynamic PSF, P_*; and g_* denotes the gradient of the latent and blurred image in all directions, respectively.

We call the first item in Eq. (10) the gradient fidelity term, which ensures the similarity of the gradient between the blurred image and latent image. The second item is called the smooth term, which ensures that there is no mutation in the blur kernel. The third item is called the numerical fidelity term, which ensures the consistency of the estimated and observed light vein pattern. According to Cho's approach, P_* can be calculated as follows. First, a bilateral filter is used to suppress the noise in the blurred image. Then a shock filter is used to enhance the edge. Finally, a strong gradient suppression is used to further remove the isolated noise. In our approach we set $\alpha = \beta = 5$.

In the third item of Eq. (10), we use P_b to estimate dynamic PSF. First we convolve the source spot S_b with current dynamic PSF, which is labeled as h_d; then we calculate the subtraction patch of the convolution result and P_b; and lastly we add up all the pixels of the subtraction patch. A smaller value of this item indicates that the estimated light vein by the model is more close to the actual light vein, which means that h_d is more accurate.

Another problem is raised: how to determine the value of r_b and l_b.

We realized that l_b is the gray value of the light source reflected to the imaging plane, which could be approximated by the average value of the light vein. Thresholding P_b using the corresponding T_b to get the binary image Q_b, and l_b can be calculated as

$$l_b = \mathrm{mean}(P_b(x, y) | \forall\ Q_b(x, y) = 1). \tag{12}$$

Equation (12) denotes that for the pixels in Q_b with a value of 1, calculate their average value in the corresponding coordinates of P_b and regard it as the intensity of S_b. The thresholding process reduces the influence of the background, while averaging weakens the isolated noise. Therefore, the estimated value of the formula is credible.

r_b denotes the radius of S_b and can be calculated as

$$r_b = \mathrm{round}\left(NT_{ij}/\sqrt{2N_{ij}}\right). \tag{13}$$

Equation (10) can be rewritten as

$$f_b(\mathbf{h_d}) = \|\mathbf{A}\mathbf{h_d} - \mathbf{b}\|^2 + \alpha\|\mathbf{h_d}\|^2 + \beta\|\mathbf{S}\mathbf{h} - \mathbf{p}\|, \tag{14}$$

where $\mathbf{h_d}$, $\mathbf{A}$, $\mathbf{b}$, $\mathbf{S}$, $\mathbf{p}$ are vectors. In order to calculate $\mathbf{h_d}$, compute the derivative of f_b with respect to $\mathbf{h_d}$ as follows:

$$\frac{\partial f_b(\mathbf{h_d})}{\partial \mathbf{h_d}} = 2\mathbf{A}^T\mathbf{A}\mathbf{h_d} + 2\beta\mathbf{h_d} - 2\mathbf{A}^T\mathbf{b} + 2\mathbf{S}^T\mathbf{S}\mathbf{h_d} - 2\mathbf{S}^T\mathbf{p} = \mathbf{0}. \tag{15}$$

By solving the equation above we can get the estimation of $\mathbf{h_d}$, or, in other words, dynamic PSF.

5. FRAMEWORK OF RESTORATION

In the content above, we have already obtained the system's static and dynamic PSFs, and the PSF of the whole imaging process is

$$h = \mathrm{PSF}_{\mathrm{static}} * \mathrm{PSF}_{\mathrm{dynamic}}. \tag{16}$$

The energy function is defined as

$$f_f(f) = \sum_{\partial_*} \omega_* \|h * \partial_* f - \partial_* g\|^2 + \gamma\|\nabla f\|^2, \tag{17}$$

where $\omega_* = \{\omega 1, \omega 2, \omega 3\}$ is the weighted gradient coefficient, and $\partial_* = \{\partial_o, \partial_x, \partial_y, \partial_{xx}, \partial_{xy}, \partial_{yy}\}$ denotes the calculating gradient in the corresponding direction. Guidance in selecting the typical value of ω_* is provided in [15]. The first item in Eq. (17) includes the numerical and gradient fidelity terms, which ensure the similarity of the gray value and gradient between the degraded and latent images. The second item is a regular smooth term, which ensures the gradient smoothing of the deblurred image. By minimizing the energy function we can get the estimated deblurred image. Compared with the

approaches in [1,8], the proposed method has a simpler calculation. After bilateral filter and shock filter in the blur kernel estimation process, the noise and ringing artifacts are effectively eliminated.

At this point, the main restoration process is finished. But the quality of the restored image could be improved by an iterative framework. To update the parameters of S_b, we define an energy function as

$$f_{S_b}(r_b, l_b) = \|S_b * h - P_b\|^2 + \|S_b - f_b\|^2. \quad (18)$$

By minimizing the energy function, we can get an updated value of r_b and l_b in each iteration.

There are three steps included in an iteration. First, the PSF of the whole system is calculated by Eqs. (15) and (16), during which the static part is fixed and the dynamic part is updated. Then based on h, S_b is updated by minimizing Eq. (18); finally, the restored image is calculated by minimizing Eq. (17). After a few iterations, we can get a restoration image with satisfactory contrast and details.

6. EXPERIMENT

A. Experimental Results

We implement our approach in MATLAB and conduct experiments on a PC with 3.4 GHz Core i7 CPU and 16 GB RAM. For evaluating the performance of our approach, an image quality metric is needed. As the reference image cannot be obtained, reference-based image quality assessments such as PSNR and SSIM [16] are not suitable here. We choose information capacity (IC) [17] as the metric of the restoration methods, which is defined as a statistical description of the pixel relativity:

$$\mathrm{IC} = \log_2\left\{1 + \sum_w \frac{\log[p(i,j,d,\theta)]}{\log[\max(p(i,j,d,\theta))]}\right\}, \quad (19)$$

where d and θ denote the relative distance and angle between pixels whose gray value is, respectively, i and j; and p denotes the relativity between the pixels. The larger the IC is, the more information the image takes. So we hope that the IC of the restoration image is larger than that of the degraded image.

We chose a tower at a distance of 3.0 km, a roof at a distance of 3.5 km, and a building at a distance of 2.8 km from the imaging system as the targets. We illuminated them, respectively, with a laser power of 35 mJ. Due to the divergence angle of the laser beam (4 mrad), the images are cropped to 150 × 150 pixels, which are shown in Fig. 3. As we can see, the edges of the roof, tower, and building are seriously blurred, and speckle noise distributes uniformly in the field of view. We compared our approach with state-of-the-art restoration methods [2,4,5,8,9]. The results are shown in Figs. 4(a)–4(f), and IC values are listed in Table 1.

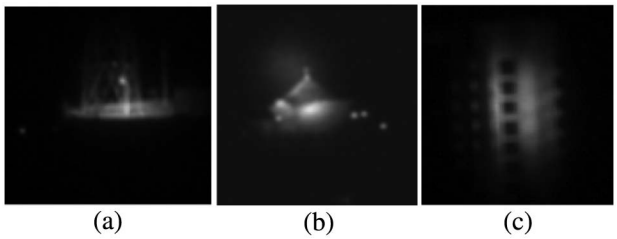

Fig. 3. Degraded image of (a) tower at distance of 3.0 km, (b) roof at distance of 3.5 km, and (c) building at distance of 2.8 km.

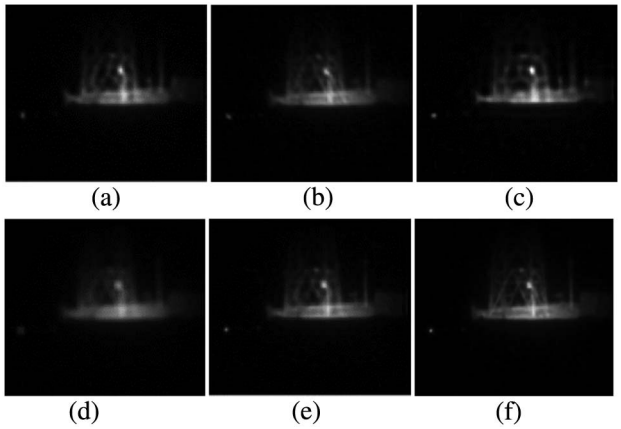

Fig. 4. Restored image of tower by (a) Fergus's method, (b) Shan's method, (c) Cho's method, (d) Goldstein's method, (e) Tai's method, and (f) proposed method.

The image quality in a range-gated imaging system is strongly associated with laser power. In order to verify the adaptability of the algorithm, we changed the laser power and evaluated the restoration results, as shown in Fig. 7.

B. Discussion

Figures 4(a), 5(a), and 6(a) illustrate that the joint MAP method by Fergus leads to unfavorable results with severe ringing artifacts, which may be attributed to the difficulty of calculating the gradient distribution model in conditions of weak light and the lack of strong constraint. In Shan's method, the ringing artifacts are effectively suppressed. However, due to the imposed contrast constraint in fuzzy parts, the restored image is not sharp enough overall. In Cho's method, which is based on edge prediction, the ringing artifacts appear in some edges because of inaccurate edge estimation, as is shown in Figs. 4(c), 5(c), and 6(c). Meanwhile, the result suffers from fake edges near the speckle spot, which leads to larger errors in kernel estimation. Goldstein's method also suffers from ringing artifacts and fuzzy edges due to the extremely high sensitivity of noise. In Tai's results, we can hardly find ringing artifacts, but fuzzy edges still exist, as is shown in Figs. 4(e), 5(e), and 6(e). In Tai's approach, denoising and kernel estimating are simply separated into two steps in every single iteration; the denoising process would bring larger errors to the kernel estimation. Visually, thanks to the accurate model of PSF, the restored image by our proposed method has few ringing artifacts, better details, and higher contrast. In Table 1, the IC values of the proposed method are higher than others, which shows the advantage of combining static and dynamic PSF, which leads to better kernel estimation.

As is shown in Fig. 7, the proposed algorithm performs best in conditions of different laser power. This can be explained by that the laser power is included as a parameter in our static PSF, and it brings the adaptability of our model. The experimental results have proved that compared with other state-of-the-art method, the proposed method is more suitable for image restoration in range-gated imaging systems.

Table 1. IC Values of Restored Images Using Different Methods

	Degraded image	Fergus's	Shan's	Cho's	Goldstein's	Tai's	Our's
tower	0.3826	0.6874	0.8055	0.7712	0.5635	0.6849	0.9125
roof	0.2579	0.5988	0.7236	0.6654	0.4312	0.4655	0.8268
building	0.4178	0.6623	0.7865	0.6497	0.5937	0.6821	0.9079

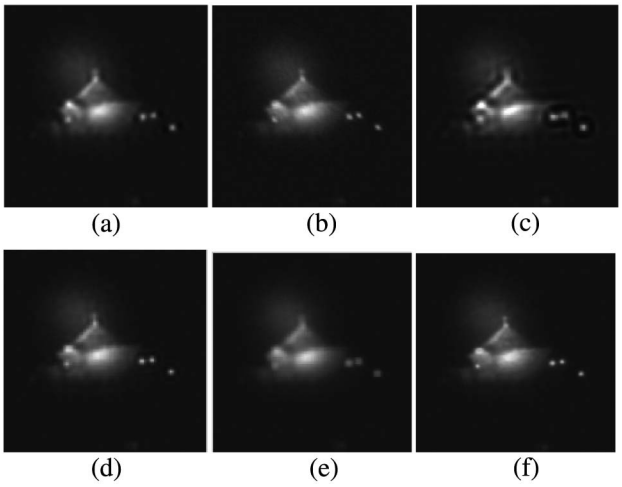

Fig. 5. Restored image of roof by (a) Fergus's method, (b) Shan's method, (c) Cho's method, (d) Goldstein's method, (e) Tai's method, and (f) proposed method.

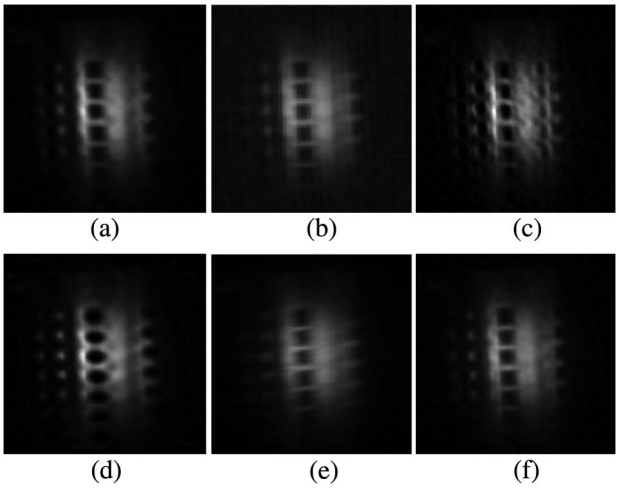

Fig. 6. Restored image of building by (a) Fergus's method, (b) Shan's method, (c) Cho's method, (d) Goldstein's method, (e) Tai's method, and (f) proposed method.

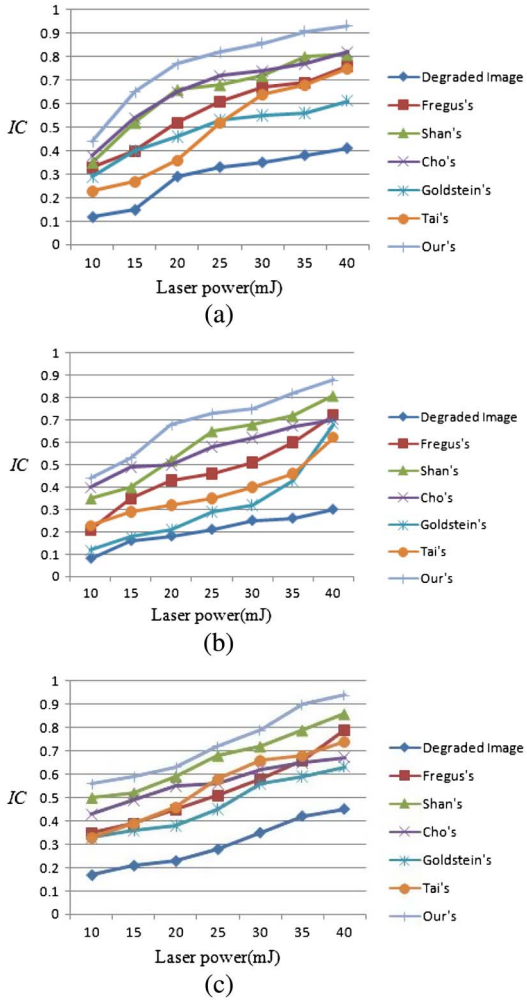

Fig. 7. IC values of (a) tower, (b) roof, (c) building in different laser power. IC increases with the laser power, and the values of our approach are far larger than those of others.

7. CONCLUSION

Due to low contrast, high noise, and fuzzy edges, traditional edge/gradient-based restoration methods cannot achieve satisfactory performance in range-gated imaging systems. In this paper, a new degradation model that contains both static and dynamic factors is proposed. The static PSF is established by considering atmospheric transmission, diffraction limit, and distortion of the sensor, and the dynamic PSF is established by proposed light vein features. Finally, the static and dynamic PSF are combined together, and image restoration is performed under an iterative framework. The proposed PSF model contains the main factors of image degradation in a laser active imaging system, which overcomes the defects of the existing algorithms based on gradients or edges, so that it can achieve good performance in the system. By changing the parameters, the proposed algorithm can also be extended to underwater laser imaging systems. Due to the small viscosity coefficient of gas, atmospheric turbulence will affect the quality of the laser beam. Because the trajectory of fluid particles is complex and

irregular, the atmospheric turbulence is not contained in our model. We will try to take it into account in our future work.

Funding. Science and Technology Development Program of Jilin, China (2013270).

Acknowledgment. The authors thank the reviewers for their valuable comments and suggestions that improve the presentation of this paper.

REFERENCES

1. J. F. Cai, H. Ji, C. Liu, and Z. Shen, "Framelet-based blind motion deblurring from a single image," IEEE Trans. Image Process. **21**, 562–572 (2012).
2. S. Cho and S. Lee, "Fast motion deblurring," ACM Trans. Graph. **28**, 145–152 (2009).
3. D. Krishnan, T. Tay, and R. Fergus, "Blind deconvolution using a normalized sparsity measure," in *Proceedings of the Computer Vision and Pattern Recognition (CVPR)*, Providence, Rhode Island, 2011, pp. 233–240.
4. R. Fergus, B. Singh, A. Hertzmann, S. T. Roweis, and W. T. Freeman, "Removing camera shake from a single photograph," ACM Trans. Graph. **25**, 787–794 (2006).
5. Q. Shan, J. Jia, and A. Agarwala, "High-quality motion deblurring from a single image," ACM Trans. Graph. **27**, 73 (2008).
6. L. Xu, S. Zheng, and J. Jia, "Unnatural l0 sparse representation for natural image deblurring," in *Proceedings of the IEEE Conference on Computer Vision and Pattern Recognition (CVPR)*, Portland, USA, 2013, pp. 1107–1114.
7. L. Yuan, J. Sun, L. Quan, and H. Y. Shum, "Image deblurring with blurred/noisy image pairs," ACM Trans. Graph. **26**, 1 (2007).
8. A. Goldstein and R. Fattal, "Blur-kernel estimation from spectral irregularities," in *European Conference on Computer Vision*, Firenze, Italy, 2012, pp. 622–635.
9. Y. W. Tai and S. Lin, "Motion-aware noise filtering for deblurring of noisy and blurry images," in *Proceedings of the Computer Vision and Pattern Recognition (CVPR)*, Providence, Rhode Island, 2012, pp. 17–24.
10. Y. Chen, W. Li, M. Xia, and K. Yang, "Model-based restoration and reconstruction for underwater range-gated imaging," Opt. Eng. **50**, 113203 (2011).
11. P. C. Ying and Z. Tao, "Signal-to-noise ratio model of laser active imaging system," Opt. Precis. Eng. **16**, 319–324 (2008).
12. N. Meitav, E. N. Ribak, and S. Shoham, "Point spread function estimation from projected speckle illumination," Light Sci. Appl. **5**, e16048 (2016).
13. M. J. Booth, "Adaptive optical microscopy: the ongoing quest for a perfect image," Light Sci. Appl. **3**, e165 (2014).
14. W. Hou, D. J. Gray, A. D. Weidemann, G. R. Fournier, and J. L. Forand, "Automated underwater image restoration and retrieval of related optical properties," in *IEEE International Geoscience and Remote Sensing Symposium*, Barcelona, Spain, 2007, pp. 1889–1892.
15. O. Whyte, J. Sivic, and A. Zisserman, "Deblurring shaken and partially saturated images," Int. J. Comput. Vis. **110**, 185–201 (2014).
16. A. Hore and D. Ziou, "Image quality metrics: PSNR vs. SSIM," in *20th International Conference on Pattern Recognition (ICPR)*, Istanbul, Turkey, 2010, pp. 2366–2369.
17. H. Han, X. Zhang, and W. Ge, "Performance evaluation of underwater range-gated viewing based on image quality metric," in *9th International Conference on Electronic Measurement & Instruments*, Beijing, China, 2009, pp. 4-441–4-444.